RSC Advances

Sonochemistry-synthesized CuO nanoparticles as anode interfacial material for efficient and stable polymer solar cells

Journal:	*RSC Advances*
Manuscript ID:	RA-ART-01-2015-000982.R1
Article Type:	Paper
Date Submitted by the Author:	15-Mar-2015

Complete List of Authors:	Zhang, Jun; Changchun Institute of Applied Chemistry, Wang, Jiantai; Changchun Institute of Applied Chemistry, Fu, yingying; Changchun Institute of Applied Chemistry, Zhang, Baohua; Changchun Institute of Applied Chemistry, ; Changchun Institute of Applied Chemistry, Chinese Academy of Sciences, State Key Laboratory of Polymer Physics and Chemistry Xie, Zhiyuan; Changchun Institute of Applied Chemistry,

The table of contents

Solution-processible CuO nanoparticles were prepared via sonochemistry and applied as anode interfacial layer to fabricate high-performance polymer solar cells.

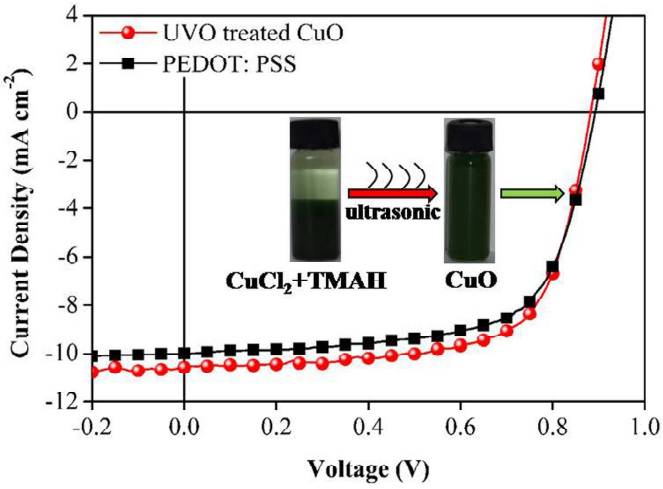

Sonochemistry-synthesized CuO nanoparticles as anode interfacial material for efficient and stable polymer solar cells

Jun Zhang,[ab] Jiantai Wang,[ab] Yingying Fu,[a] Baohua Zhang,[a] and Zhiyuan Xie[a,*]

[a]*State Key Laboratory of Polymer Physics and Chemistry, Changchun Institute of Applied Chemistry, Chinese Academy of Sciences, Changchun 130022, P. R. China.*

[b]*University of Chinese Academy of Sciences, Beijing 100049, P. R. China.*

*corresponding author: E-mail: xiezy_n@ciac.ac.cn

Submitted to *RSC Advances*

ABSTRACT:

Solution-processible copper oxide (CuO) nanoparticles have been synthesized via sonochemistry. Colloidal crystalline CuO nanoparticles with diameters of 3-12 nm were obtained from the $CuCl_2$ metal salt at low temperature under ultrasound irradiation. The solution-processible CuO nanoparticles are applied as anode buffer layer in PCDTBT:$PC_{71}BM$ bulk heterojunction solar cell to substitute the commonly used hygroscopic PEDOT:PSS. It is found that UV-Ozone treatment increases the work function of CuO buffer layer from -4.7 to -5.4 eV, facilitating with the interfacial contact and hole extraction. The UVO-treated CuO-based solar cells show enhanced fill factor and photocurrent, resulting in an increased photovoltaic performance from 6.00% to 6.44% in comparison to the PEDOT:PSS-based solar cells. Moreover, the solar cells with CuO buffer layer show better ambient stability than those with PEDOT:PSS buffer layer. The facile preparation of solution-processed CuO and effectiveness in polymer solar cells render it a promising anode interfacial material for solution-processed flexible polymer solar cells.

Keywords: polymer solar cell, solution-processible, CuO nanoparticles, anode interfacial layer, sonochemistry.

1. Introduction

Polymer solar cells (PSCs) are a promising low-cost renewable energy source that are compatible with flexibility, cleanness and low-temperature solution processing compared to traditional inorganic solar cells.[1-4] Over the past decades, along with the advances of novel low bandgap polymer donors toward improving the spectral coverage to solar light and the rational device design as well as morphology control to improve the photovoltaic performance, the power conversion efficiency (PCE) of PSCs has reached the so-called threshold of 10%, giving hope for PSCs to be brought to market.[5,6] In addition to the PCE values, the stability and the large-area solution processibility are equally important for the future application of PSCs. Improving the intrinsic stability of PSCs is necessary for practical applications since most low-cost encapsulation technologies offer only limited protection against oxygen and water ingress. The common PSCs have a sandwich structure with the active layer comprising polymer donor and fullerene acceptor bulk heterojunction between the two electrodes. The interfacial layers are usually inserted between the electrodes and the active layer to facilitate interfacial contact and improve selective charge extraction.[7-9] Poly(3,4-ethylenedioxythiophene):poly (styrene sulfonate) (PEDOT: PSS) has been the most popular anode buffer material due to its high work function, high conductivity and favorable solution processibility. However, the highly acidic PEDOT:PSS has been assumed to etch the undereath indium tin oxide (ITO) electrode and consequently degrade the device stability.[10] The hygroscopic nature of PEDOT:PSS also has a detrimental impact on the device lifetime.[11,12] In 2013, Shao *et*

al. developed a solution-processed neutral and less hygroscopic anode interfacial layer MoO_3-PEDOT:PSS by in situ formation of MoO_3 in aqueous PEDOT:PSS dispersion and the resulted PSC showed considerably improved stability compared with the reference pristine PEDOT:PSS-based device.[13] These works highlight the necessity to develop new anode interfacial materials to substitute PEDOT:PSS.

The potential substituents of PEDOT:PSS should possess high transparency, high work function, excellent ambient stability and solution-processibility compatible with low-cost and large-area roll-to-roll production for PSCs. Transition metal oxides have been promising candidates to substitute PEDOT:PSS due to their good environmental stability, high optical transparency and facile synthysis.[14,15] Some solution-processed high work function transition metal oxides, such as MoO_3,[16-18] V_2O_5,[19,20] and NiO[21-24] have been used to substitute PEDOT:PSS as anode interfacial layers to fabricate photovoltaic devices, since Liu *et al*. for the first time reported a solution-processed MoO_3 to replace PEDOT:PSS in PSCs.[25] However, these solution-processible transition metal oxides films prepared from sol-gel chemistry required high temperature annealing (>150˚C) to realize high photovoltaic performance. More recently, solution-processible crystalline NiO nanoparticles were prepared via sonochemical synthesis and were successfully applied as the anode interfacial layer in low-temperature-annealing PSCs, which provided a new approach to prepare solution-processible transition metal oxides interfacial materials for PSCs.[26]

Copper oxide (CuO) is a kind of p-type semiconductor. Compared with other transition metal oxides, CuO has some potential advantages including earth-abundant

source, low cost and nontoxicity. p-type CuO having a high concentration of Cu vacancies and stable defects under O-rich conditions is able to facilitate the contact with ITO anode. There were some attempts to use solution-processed CuO prepared with sol-gel chemistry as anode interfacial layer in PSCs.[27,28] Herein, Solution-processible CuO nanoparticles are synthesized at low temperatures via sonochemistry. The solution-processible CuO nanoparticles are applied as anode buffer layer in PCDTBT:$PC_{71}BM$ bulk heterojunction solar cell to substitute the commonly used hygroscopic PEDOT:PSS. The CuO-based PSC shows not only enhanced photovoltaic performance with PCE increased from 6.00% to 6.44%, but also improved ambient stability compared with the reference device based on the PEDOT:PSS anode buffer layer.

2. Experimental section

Materials. The poly[N-9''-hepta-decanyl-2,7-carbazole-alt-5,5-(4',7'-di-thienyl-2',1',3'-benzothiadiazole)] (PCDTBT) with a weight-average molecular weight of 24000 and a polydispersity index of 1.8 was synthesized in our laboratory. [6,6]-phenyl C71-butyric acid methyl ester ($PC_{71}BM$, >99%) was purchased from Solarmer Energy Inc. and used as received. The aqueous solution of PEDOT:PSS (Clevios P VP AI 4083) was obtained from Heraeus and filtered with a 0.45 μm PTFE filter before use. Anhydrous 1, 2-dichlorobenzene was obtained from Aldrich Co. and purged with nitrogen in order to remove residual oxygen prior to use. $CuCl_2$ was of analytical purity and was used as received from Shanghai Chemical Company.

Synthesis of CuO nanoparticles. Solution-processible CuO nanoparticles were

synthesized according to the previously reported synthesis of NiO nanoparticles.[26] The metal salt $CuCl_2$ was dissolved in ethanol with a concentration of 0.01 M and the solution was kept at 80˚C for 30 minutes. Then, tetramethylammonium hydroxide (TMAH) was added into the $CuCl_2$ solution and the pH value of the final suspension was adjusted to about 10. The mixture solution was stirred at room temperature for one hour. Subsequently, the mixture solution was exposed to high-intensity ultrasonic irradiation (6 mm diameter Ti-horn, 300 W, 20 kHz) at room temperature under ambient conditions for 45 min. Finally, the supernatant was removed and the resulting dispersion in ethanol was centrifuged at 5000 rpm for 3min. The product was dispersed again in ethanol at a concentration of 4 mg mL^{-1} by ultrasonication. The ethanol sol of CuO nanoparticles was readily obtained. The solution-processible CuO were also prepared with sol-gel chemistry as reported for comparison studies.[28]

Thin film characterization. The thickness of various films was measured with a Dektak 6M Stylus Profiler. Optical transmission spectra of various samples were recorded on a UV-Vis spectrophotometer. The ultraviolet photoelectron spectroscopy (UPS) and X-ray photoelectron spectroscopy (XPS) measurements were carried out using a Thermo ESCALAB 250. Monochromatized Al Ka (*hv*= 1486.8 eV) excitation and a He-I (21.2 eV) discharge lamp were used for the XPS and UPS measurements, respectively. For UPS measurement, a sample bias of 10 V was applied in order to separate the sample and the secondary edge for the analyzer. The transmission electron microscopy (TEM) samples were prepared by drop-casting the diluted sol solution of CuO nanoparticles onto a copper grid, and imaged using a FEI TECNAI

F20 system operated at a working voltage of 200 kV. The atomic force microscopy (AFM) images were obtained using a SPA-300HV instrument with a SPI3800N Controller (Seiko Instruments Inc., Japan) in tapping mode.

Fabrication and measurement of PSCs. The patterned ITO-coated glass substrates were cleaned with routine process and were dried at 120˚C in an oven overnight. The cleaned ITO substrates were subject to UV-Ozone treatment for 30 min before use. For the control cell with PEDOT:PSS buffer layer, the aqueous PEDOT:PSS solution was spin-coated onto the ITO glass substrate to produce a 30-nm-thick PEDOT:PSS buffer layer and was subject to thermal annealing on a hot plate at 130˚C for 30 minutes. For the PSCs with CuO as anode buffer layer, the ethanol sol of CuO nanoparticles with a concentration of 4 mg mL^{-1} was deposited on the ITO glass substrate via spin coating at a spin rate of 400 rpm for 15 s, and then the samples were subject to thermal annealing at 60˚C for 10 min to remove the residual ethanol solvent. The thickness of obtained CuO nanoparticles film is about 15 nm as measured by the stylus profiler. The CuO-coated substrates were subject to UV-Ozone treatment for 30 min before depositing the active layer. A solution comprising PCDTBT and $PC_{71}BM$ (1:4 in weight) was prepared in an inert atmosphere with a total concentration of 17.5 mg mL^{-1} in 1,2-dichlorobenzene. The solution was stirred at 90˚C for at least two hours and was kept overnight before use. The PCDTBT:$PC_{71}BM$ solution in 1,2-dichlorobenzene was spin-cast on top of the PEDOT:PSS or CuO layers at a spin rate of 600 rpm to produce ca. 80-nm-thick active layers. Subsequently, the samples were transferred into a vacuum chamber and a cathode structure of LiF(0.5 nm)/Al

(100 nm) was thermally evaporated at a base pressure of 4×10^{-6} Torr. The active area of the cells was about 16 mm^2 defined by the overlapping area of the ITO and Al electrodes. An Oriel solar simulator with an AM 1.5G filter was used to provide an intensity of 100 mW cm^{-2} for illumination of the photovoltaic cells. The light intensity was determined by using a calibrated silicon diode with a KG-5 visible color filter. Current density-voltage (J-V) traces were obtained with a Keithley 236 source meter. The external quantum efficiency (EQE) measurement was performed under short circuit conditions using Enlitech QE-R equipment.

3. Results and discussion

Herein, we prepared CuO nanoparticles sol via a simple sonochemical synthesis. Ultrasonic irradiation can promote the sol-gel processes under normal temperature to attain nanostructured metal oxides in an extreme physical environment posed by the acoustic cavitation effect. At the interfaces between a collapsing bubble and the bulk solution an extreme physical environment with a high temperature of ~1900 K can be created.[29,30] The metal salt $CuCl_2$ first reacted with the alkali (TMAH) to get a $Cu(OH)_2$ suspension. Under ultrasonic irradiation conditions, the suspension precursor was converted into crystalline CuO nanoparticles at the interfaces between the bubbles and the bulk solution. The bulk solution temperature remains approximately constant at room temperature during the sonochemical synthesis. In contrast to the common sol-gel synthesis of metal oxides, this process can completely avoid the required high temperature post-annealing and is compatible with flexible substrates and low-cost high-throughput fabrication. Figure 1 shows the

low-magnification and high-magnification TEM images of the as-synthesized CuO nanoparticles. We can see that the CuO nanoparticles with diameters of 3–12 nm are readily prepared. The selected-area electron diffraction (SAED) pattern of the synthesized CuO nanoparticles is shown in the inset of Fig.1(a). The SAED pattern indicates that the CuO nanoparticles prepared with sonochemical method are polycrystalline. The high-resolution TEM image of one CuO nanoparticle is shown in the inset of Fig. 1(b). A periodic lattice spacing of 2.3 Å can be assigned to the (111) planes of crystalline CuO nanoparticles.[31] These data indicate that the crystalline CuO nanoparticles are successfully prepared at low temperatures via sonochemical synthesis.

The XPS measurement was carried out to explore the changes of chemical component of the as-synthesized CuO nanoparticles before and after UV-Ozone treatment. The peaks for the Cu $2p_{3/2}$ spectrum are used to analyze surface Cu component. Figure 2 shows the peak fit of Cu $2p_{3/2}$ core level and its corresponding shake-up satellites for the as-deposited and UVO-treated CuO nanoparticle films. The XPS peaks were fitted mathematically using the overlapping Lorentzian (80%)-Gaussian (20%) profiles. The XPS spectra are corrected by the C 1s peak of 284.8 eV. It can be seen that both as-deposited and UVO-treated CuO nanoparticles are composed of a mixture of Cu^{1+} and Cu^{2+} ions. The Cu $2p_{3/2}$ peak positioned at 932.5 eV is assigned to the Cu^{1+} state and the peak positioned at 934.1 eV is assigned to the Cu^{2+} state. The additional peaks around 940 eV in the Cu $2p_{3/2}$ peak region is considered to originate from a shake-up process due to the open $3d^9$ shell of Cu^{2+}.[32]

UV-ozone treatment further oxidizes the as-deposited CuO nanoparicles. We can see that the intensity of Cu^{2+} in the UVO-treated CuO nanoparticles film is apparently higher than that of Cu^{1+} compared to the as-deposited CuO nanoparticles. For the p-type metal oxide semiconductors, a considerable concentration of the free holes exists in the valence band. The concentration of the free holes is mainly determined by the metal deficit or excess oxygen concentration within the crystallite sites of the materials. This phenomenon is attributed to the deviation from the stoichiometric composition of the components, which is closely related to the preparation condition of the material.[33,34] Herein, the UV-Ozone treatment of CuO nanoparticles can increase oxygen concentration and the content of Cu^{2+} ions, thus having potential to tune its work function and improve its conductivity.

The work function of the CuO nanoparticles is assumed to be strongly dependent on its surface chemical composition. The work function changes of CuO nanoparticles after UV-Ozone treatment is detected by the UPS measurement. The UPS spectra at high binding energy region for the as-deposited and UVO-treated CuO nanoparticles are plotted in Figure 3(a), from which the work function of CuO nanoparticles can be deduced with work function = photon energy (21.2 eV)—high binding energy cutoff. The as-deposited CuO nanoparticles film gives a relatively work function of -4.7 eV. When the as-deposited CuO nanoparticles film is subject to the UVO-Ozone treatment for 30 min, its work function is increased to about -5.4 eV. The UPS spectra at low binding energy region for the as-deposited and UVO-treated CuO nanoparticles are shown in Figure 3(b). The valence band maximum (VBM) associated with

ionization energy for the as-deposited and UVO-treated CuO nanoparticles appear at 1.1 and 0.7 eV, respectively, with respect to the fermi level. Thus, the VBMs of the as-deposited and UVO-treated CuO namoparticles are estimated to be -5.8 eV and -6.1 eV, respectively, with respect to the vacuum level. Compared to that of the as-deposited CuO nanoparticles, the fermi level of UVO-treated CuO nanoparticles shifts to the valence band, indicating an enhanced p-type semiconductor characteristic of the CuO nanoparticles after UV-Ozone treatment. These changes of work function and p-type semiconductor characteristics of the synthesized CuO nanoparticles are originated from the increased contents of Cu^{2+} ions after UV-Ozone treatment. The increased work function and enhanced p-type semiconducting characteristics of UVO-treated CuO nanoparticles are helpful to facilitate the contact with the HOMO of polymer donor in the active layer and enhance the hole extraction when it is used as the anode interfacial layer in PSCs.

The optical property and film morphology of the CuO nanoparticles film used in PSCs are further investigated. The preparation conditions for the samples are the same as the device fabrication. Figure 4 shows the optical transmittance spectra of the samples having structures of glass/ITO/PEDOT:PSS, glass/ITO/as-deposited CuO and glass/ITO/UVO-treated CuO, with a blank glass as reference. In comparison to the reference glass/ITO/PEDOT:PSS sample, the glass/ITO/CuO samples show higher transmittance at 500-800 nm region. However, the transmittance of CuO-based samples at 400-500 nm is decreased compared to the PEDOT:PSS-based sample. UV-Ozone treatment of CuO nanoparticles film further increases its transmittance in

the longer wavelength range. AFM measurement is used to investigate the surface morphology of the CuO nanoparticle films. The thickness of the CuO nanoparticles is about 15 nm as measured by the stylus profiler. Figure 5 presents the height and phase images of the as-deposited and UVO-treated CuO nanoparticle films. From the height images, we can see that the solution-processed CuO nanoparticle films are a little coarse. The root-mean-square roughnesses of as-deposited and UVO-treated CuO films are 8.58 and 12.02 nm, respectively. The more coarse surface morphology of the UVO-treated CuO film may be originated from the penetration of oxygen atoms. However, the more uniform phase images of the as-deposited and UVO-treated CuO films indicate a full coverage of CuO on the underlying ITO electrode.

The photovoltaic cells based on PCDTBT:$PC_{71}BM$ (1 : 4 in weight) bulk heterojunction employing the solution-processed CuO nanoparticles as the anode interfacial layer were fabricated. The illuminated J-V characteristics of the PCDTBT:$PC_{71}BM$ PSCs with the as-deposited and UVO-treated CuO interfacial layers under 100 mW/cm^2 AM 1.5 simulated solar light is plotted in Figure 6(a). The control device with PEDOT:PSS interfacial layer is also given for comparison study. The series resistance (R_S) and parallel resistance (R_P) were calculated from the illuminated J-V curves near the open-circuit voltage (V_{OC}) and at around 0V, respectively. All the photovoltaic parameters of these PSCs are summarized in Table 1. The PEDOT:PSS-based control device demonstrates a V_{OC} of 0.89 V, a short-circuit current density (J_{SC}) of 10.00 mA cm^{-2}, and a fill factor (FF) of 67.20%, giving an overall PCE of 6.00%. When the as-deposited CuO is used to substitute the

PEDOT:PSS layer, the resulted device merely shows a V_{OC} of 0.59 V, a J_{SC} of 8.89 mA cm^{-2} and an FF of 35.2%, leading to a low PCE of 1.85%. This is mainly originated from the poor contact between the PCDTBT donor and as-deposited CuO due to its low work function. However, when the as-deposited CuO nanoparticle layer is subject to UV-Ozone treatment, the photovoltaic performance of the devices is greatly improved. The resulted device shows a V_{OC} of 0.89 V, a J_{SC} of 10.58 mA cm^{-2} and a FF of 68.40%, leading to a high PCE of 6.44%. The resulted J_{SC}, FF and PCE are even higher than those of the PEDOT:PSS-based devices. The improvement may benefit from the more facilitated contact between the polymer donor and the UVO-treated CuO nanoparticles due to its high work function and enhanced p-type semiconducting property. The UVO-treated CuO-based device shows the lowest R_S among the three kinds of devices. More than 20 devices for each type of cells were fabricated under the same conditions. The deviation of efficiencies for these devices is less than 5% as shown in Table 1. The EQE curves of the three kinds of PSCs are plotted in Figure 6(b). We can see that the quantum efficiencies are greatly increased after the as-deposited CuO is subject to UV-Ozone treatment. The EQE of the UVO-treated CuO-based cell is also higher than that of the PEDOT:PSS-based control device. The calculated J_{SC}s from EQE curves are 10.00, 9.00 and 10.70 mA cm^{-2}, respectively, for the PSCs using PEDOT:PSS, as-deposited CuO and UVO-treated CuO buffer layer. These values are well matched with the measured J_{SC}s of 10.00, 8.89 and 10.58 mA cm^{-2} for the corresponding devices. The PSC using solution-processed CuO prepared with sol-gel chemistry as anode interfacial layer

was also fabricated for comparison. The illuminated J-V curve and detailed photovoltaic parameters are given in Figure S1 and Table S1 in the Supporting Information. The PSC based on the sol-gel prepared CuO shows a V_{OC} of 0.89 V, a J_{SC} of 10.08 mA cm^{-2} and a FF of 62.02%, leading to a PCE of 5.56%. Compared to the PSC based on sol-gel prepared CuO, both the J_{SC} and FF are increased for the devices using sonochemistry-synthesized CuO as the anode interfacial layer. This may be originated from the enhanced charge collection capability by using the UVO-treated CuO prepared via sonochemistry as the anode interfacial layer.

The origin of the enhanced performance for the devices using UVO-treated CuO interfacial layer was further investigated by using the AC impedance spectroscopy. The impedance measurements were performed with Agilent E4980A precision LCR Meter with a 25 mV AC signal at frequencies from 20 Hz to 2 MHz. The Nyquist plots of the PSCs with different anode interfacial layers are shown in Figure 7. From these plots, the R_S of the PSCs with different anode interfacial layers were extracted according to the equivalent modeled circuit.[28,35] The R_S is assumed to consist of a interfacial contact resistance and a bulk resistance of the active layer. The calculated Rs are 10.73, 44.5 and 4.91 Ω cm^2, respectively, for the PSCs with PEDOT:PSS, as-deposited CuO and UVO-treated CuO as the anode interfacial layers. The reduced R_S should be ascribed to the improved interfacial contact between the UVO-treated CuO and the active layer, which improves the charge extraction.

The effects of UVO-treated CuO interfacial layer on the ambient stability of the cells have been investigated in comparison to the PEDOT:PSS-based control cells.

Twenty devices for each type of cells were tested without encapsulation. The average values and errors of the normalized photovoltaic parameters evolution including V_{OC}, J_{SC}, FF and PCE within 120 hours are depicted in Figure 8. In fact, both the active layer and top electrode also contribute to the overall degradation. As the active layer and top cathode structure are the same, herein it is assumed that the distinct difference of ambient stability for the two kinds of devices is originated from the effect of different anode interfacial layers. The V_{OC} and FF of the PEDOT:PSS- and CuO-based cells degrade similarly with initial 80 hours. After then, the V_{OC} and FF of the CuO-based cell keep stable while those of PEDOT:PSS-based cell degrade distinctly. The initial drop in V_{OC} for the two kinds of cells is likely due to oxidation of aluminum electrode in ambient conditions. The J_{SC} of the PEDOT:PSS-based cells shows rapid degradation compared to the CuO-based cells within 120 hours. Finally, after stored in ambient condition for 120 hours, the PCE of the CuO-based cells drops to 50% of its initial value and the degradation behaviour becomes slowly after 80 hours. However, for the PEDOT:PSS-based control devices, the PCE almost linearly drops to 30% within 120 hours. These results indicate that the ambient stability of PSCs is enhanced to some extent by using solution-processed CuO nanoparticles to substitute the commonly used PEDOT:PSS anode interfacial layer. The reason can be attributed to the less hygroscopic nature of CuO nanoparticles than the PEDOT:PSS.

4. Conclusions

In summary, solution-processible CuO nanoparticles have been synthesized via sonochemistry and used as anode interfacial layer in polymer solar cells to substitute commonly used hygroscopic PEDOT:PSS. UV-Ozone treatment of as-deposited CuO nanoparticles can increase the content of Cu^{2+} ions and improve the work function of CuO interfacial layer from -4.7 to -5.4 eV, thus facilitating with the interfacial contact

and hole extraction. The resulted PSCs show not only enhanced photovoltaic performance, but also improved ambient stability in comparison to the PEDOT:PSS-based PSCs. The facile preparation in low temperature, low cost and environmentally-friendly nature of solution-processed CuO nanoparticles and its effectiveness in polymer solar cells render it a promising anode interfacial material for solution-processed flexible PSCs.

■ AUTHOR INFORMATION

Corresponding Author

*Tel.: +86 431 8526 2819. Fax: +86 431 8526 2126. E-mail: xiezy_n@ciac.ac.cn.

Notes

The authors declare no competing financial interest.

■ ACKNOWLEDGMENTS

This work was supported by the National Basic Research Program of China (973 Project, Grant 2014CB643504), the National Natural Science Foundation of China (nos. 51325303, 51273193 and 21334006) and the Strategic Priority Research Program of the Chinese Academy of Sciences (XDB12030200). J. Zhang thanks Dr. H. B. Wang and X. L. Li for helpful discussions about the XPS and UPS measurement and relevant data analysis.

References

(1) S. Gunes, H. Neugebauer, N. S. Sariciftci, *Chem. Rev.* 2007, **107**, 1324.

(2) W. Clemens, W. Fix, J. Ficker, A. Knobloch, A. J. Ullmann, *Mater. Res*. 2011, **19**, 1963.

(3) C. J. Brabec, N. S. Sariciftci, J. C. Hummelen, *Adv. Funct. Mater.*, 2001, **11**,15.

(4) S. Gunes, H. Neugebauer, N. S. Sariciftci, *Chem. Rev.,* 2007, **2**, 145.

(5) M.C. Scharber, D. Mühlbacher, M. Koppe, P. Denk, C. Waldauf, A.J. Heeger, C.J. Brabec, *Adv. Mater*., 2006, **18**, 789.

(6) Y. H. Liu, J. B. Zhao, Z. K. Li, C. Mu, W. Ma, H. W. Hu, K. Jiang, H. R. Lin, H. Ade, H. Yan, *Nat. Commun.*, 2014, **5**, 5293 .

(7) R. Po, C. Carbonera, A. Bernardi and N. Camaioni, *Energy Environ. Sci.*, 2011, **4**, 285.

(8) R. Steim, F. R. Kogler and C. J. Brabec, *J. Mater. Chem.*, 2010, **20**, 2499.

(9) L. Ratcliff, E. B. Zacher, N. R. T. Armstrong, *J. Phys. Chem. Lett.*, 2011, **2**, 1337.

(10) M. Girtan, M. Rusu, *Sol. EnergyMater. Sol. Cells.*, 2010, **94**, 446.

(11) K. X. Steirer, J. P. Chesin, N. E. Widjonarko, J. J. Berry, A. Miedaner, D. S. Ginley, D. C. Olson, *Organic Electronics,* 2010. **11**, 1414.

(12) J. Ni, H. Yan, A.Wang, Y. Yang, C. L. Stern, A.W.Metz, S. Jin, L.Wang, T. J. Marks, J. R. Ireland, C. R. Kannewurf, *J. Am. Chem. Soc.*, 2005, **127**, 5613.

(13) S. Y. Shao, J. Liu, J. Bergqvist, S. W. Shi, C. Veit, U. Würfel, Z. Y. Xie, F. L. Zhang, *Adv. Energy Mater*. 2013, **3**, 349.

(14) M. T. Greiner, Z. H. Lu, *NPG Asia Mater.*, 2013, **5**, e55.

(15) S. Chen, J. R. Manders, S. W. Tsang, F. So, *J. Mater. Chem*., 2012, **22**, 24202.

(16) C. Girotto, E. Voroshazi, D. Cheyns, P. Heremans and B. P. Rand, *ACS Appl. Mater. Interfaces.*, 2011, **3**, 3244.

(17) S.-Y. Lin, C.-M. Wang, K.-S. Kao, Y.-C. Chen, C.-C. Liu, *J. Sol-Gel Sci. Technol.*, 2010, **53**, 51.

(18) J. J. Jasieniak, J. Seier, J. Jo, T. Mates, A. Heeger, *Adv. Funct. Mater.*, 2012, **22**, 2594.

(19) K. Zilberberg, S. Trost, H. Schmidt, T. Riedl, *Adv. Energy Mater.*, 2011, **1**, 377.

(20) H. Q. Wang, N. Li, N. S. Guldal, C. Brabec, *Org. Electron.*, 2012, **13**, 3014.

(21) J. R. Manders, S. W. Tsang, M. J. Hartel, T. H. Lai, S. Chen, C. M. Amb, F. So, *Adv. Funct. Mater.*, 2013, **23**, 2993.

(22) A. Garcia, G. C. Welch, E. L. Ratcliff, D. S. Ginley, G. C. Bazan, D. C. Olson, *Adv. Mater.*, 2012, *24*, 5368.

(23) K. X. Steirer, P. F. Ndione, N. E. Widjonarko, M. T. Lloyd, J. Meyer, E. L. Ratcliff, D. C. Olson, *Adv. Energy Mater.*, 2011, **1**, 813.

(24) Z. Zhai, X. Huang, M. Xu, J. Yuan, J. Peng, W. Ma, *Adv. Energy Mater.*, 2013, **3**, 1614.

(25) F. Liu, S. Shao, X. Guo, Y. Zhao, Z. Xie, *Sol. Energy Mater. Sol. Cells* 2010, **94**, 842.

(26) J. Zhang, J. T. Wang, Y. Y. Fu, B. H. Zhang, Z. Y. Xie, *J. Mater. Chem. C*., 2014, **2**, 8295.

(27) M.-Y. Lin, C.-Y. Lee, S.-C. Shiu, I.-J. Wang, J.-Y. Sun, W.-H. Wu, Y.-H. Lin, J.-S.

Huang, C.-F. Lin, *Org. Electron.,* 2010, **11**, 1828.

(28) Q. Xu, F. Wang, Z. A. Tan, L. Li, S. Li, X. Hou, Y. F. Li, *ACS Appl. Mater. Interfaces*, 2013, **5**, 10658.

(29) H. Xu, B. W. Zeiger, K. S. Suslick, *Chem. Soc. Rev.*, 2013, **42**, 2555.

(30) J. H. Bang, K. S. Suslick, *Adv. Mater.*, 2010, **22**, 1039.

(31) M. Estruga, A. Roig, C. Domingo, J. A. Ayllón, *Journal of Nanoparticle Research*, 2012, **14**, 1053.

(32) S. K. Małgorzata, C. Lea, N. Shieling, G. M. Haresh, H. Christopher, N. Peter, *Dalton Trans.,* 2012, **41**, 219.

(33) N. Banerjee, S. Kundoo, KK. Chattopadhyay, *Thin Solid Films*, 2003, **440**, 5.

(34) Y. Ohya, S. Ito, T. Ban, Y. Takahashi, *Key Eng Mater*., 2000,**181–182**,113.

(35) W. Kai, R. He, Y. Chao, L. Chang, W. H. Xing, H. Lin, Z. H. Li, K. Alamgir, G. Xiong, *ACS Appl. Mater. Interfaces*, 2013, **5**, 10325.

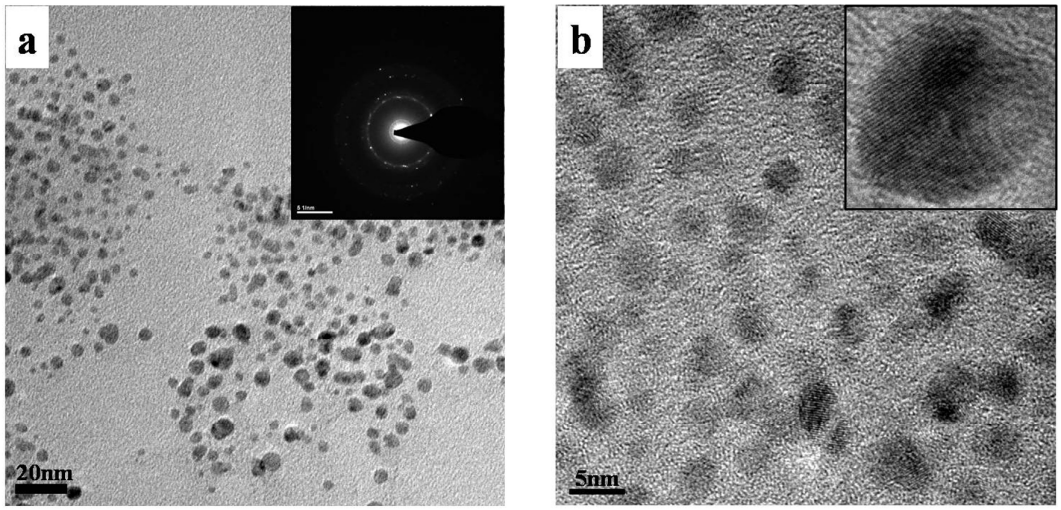

Figure 1 The low-magnification (a) and high-magnification (b) TEM images of the as-synthesized CuO nanoparticles showing typical diameters of 3–12 nm. The inset in (a) shows the SAED pattern of the CuO nanoparticles. The inset (b) shows a close-up of one CuO particle with the (111) lattice spacing of 2.3 Å.

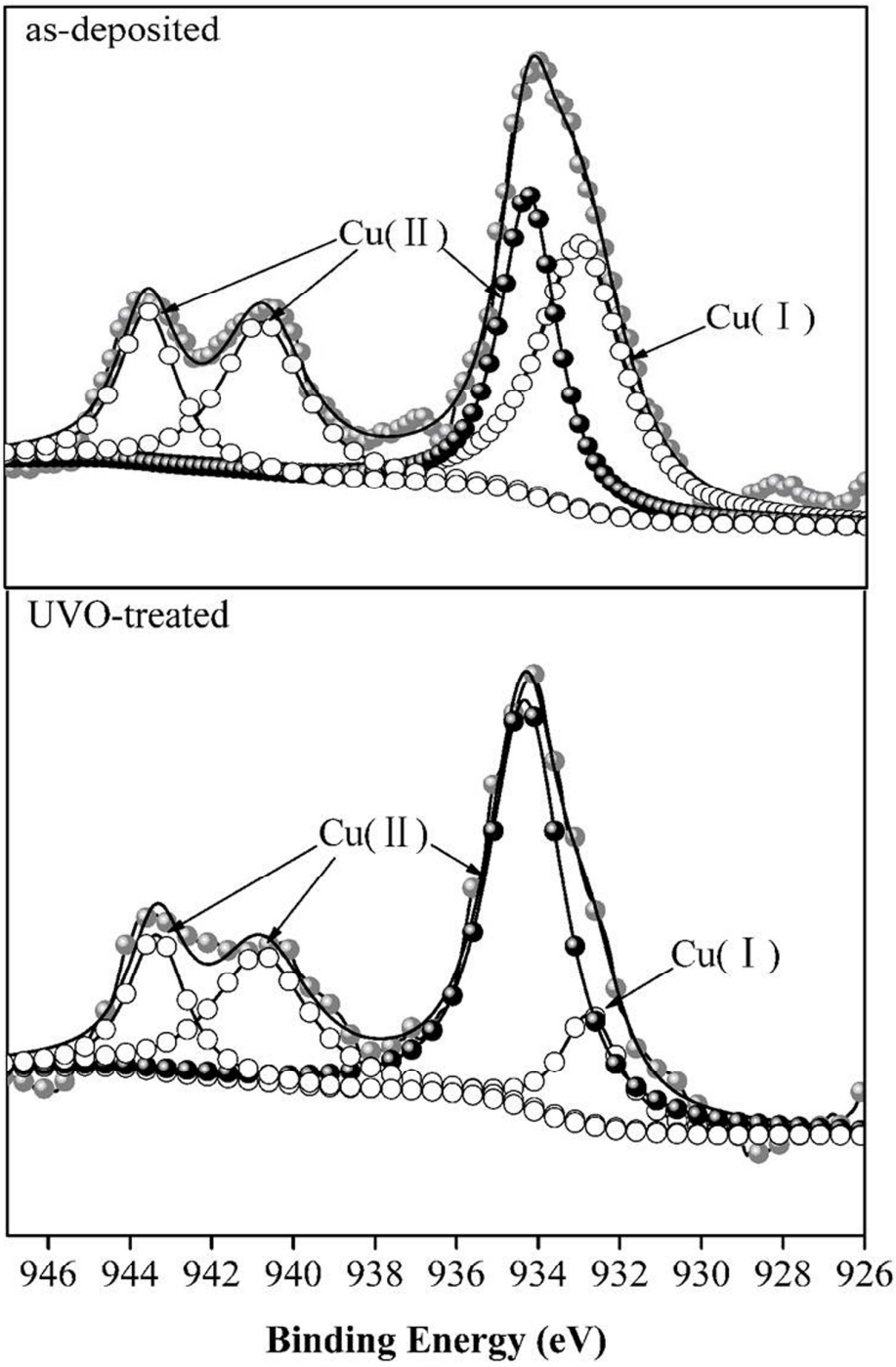

Figure 2. The Cu $2p_{3/2}$ core level peaks of the as-deposited (upper) and UVO-treated CuO films (below).

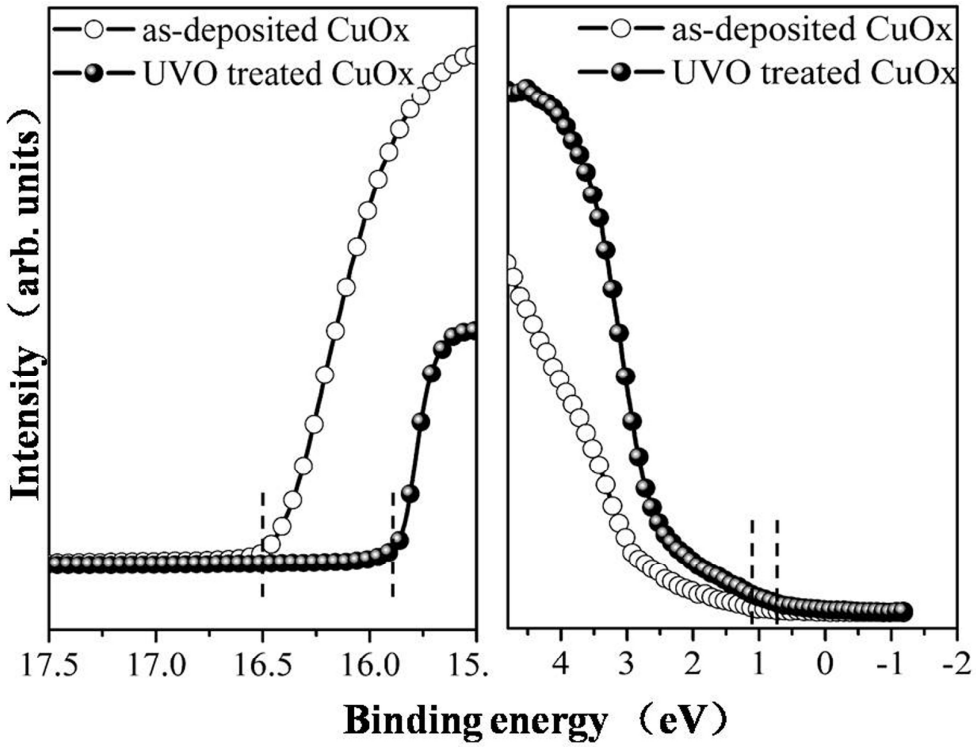

Figure 3. UPS spectra of the as-deposited and UVO-treated CuO nanoparticle films showing (a) the secondary edge at high binding energy region related to work function and (b) the low energy region related to valence band maximum.

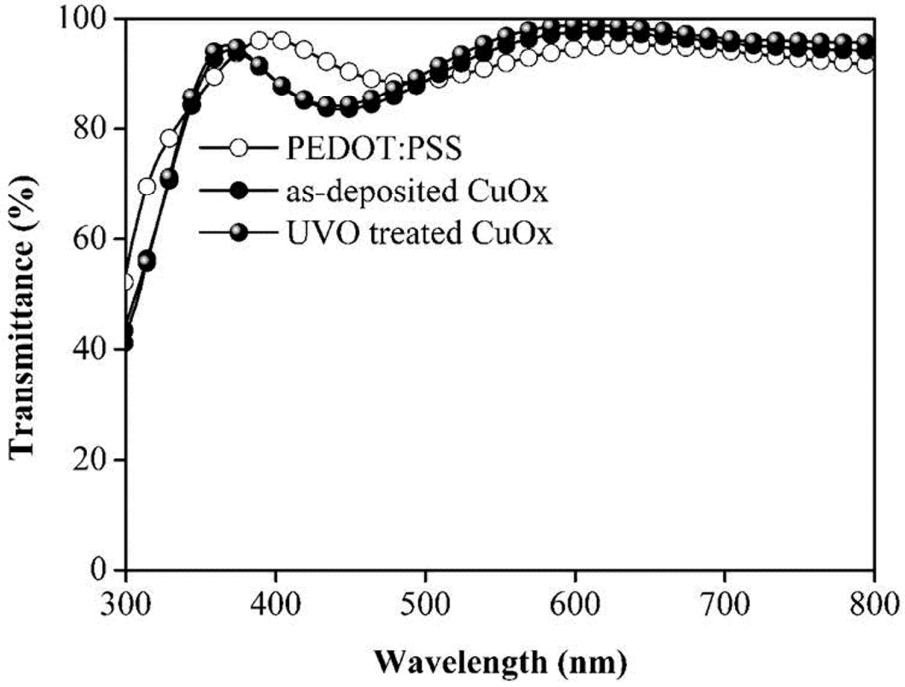

Figure 4. Optical transmittance spectra of the samples having structures of glass/ITO/PEDOT:PSS, glass/ITO/as-deposited CuOx and glass/ITO/UVO-treated CuO, with a blank glass as reference.

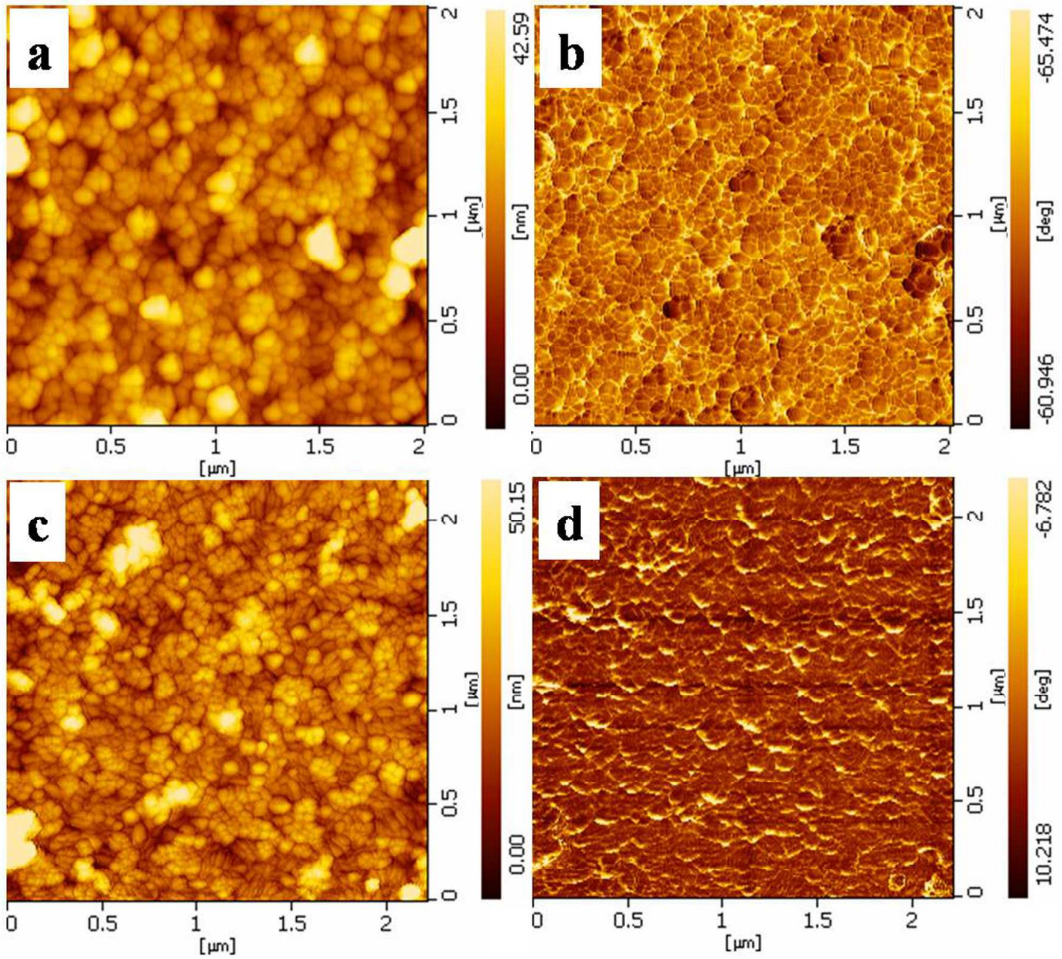

Figure 5. Tapping-mode AFM height images of the as-deposited (a) and UVO-treated (c) CuO nanoparticle films, and the corresponding phase images of as-deposited (b) and UVO- treated (d) CuO nanoparticle films.

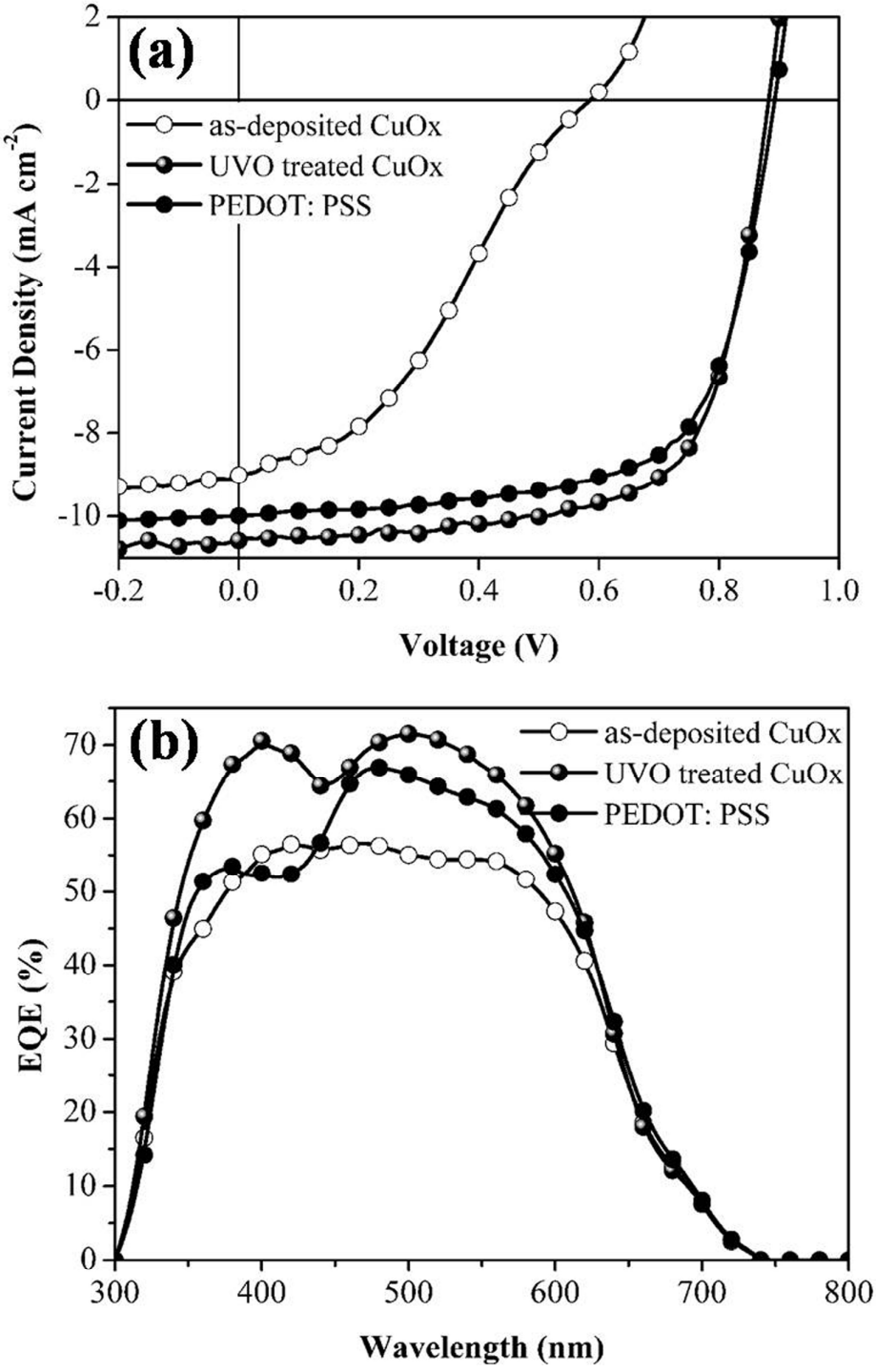

Figure 6. (a) The illuminated J-V characteristics of the PCDTBT:$PC_{71}BM$ PSCs with PEDOT:PSS, as-deposited CuO and UVO-treated CuO anode buffer layers, respectively. (b) The corresponding EQE spectra of the PSCs.

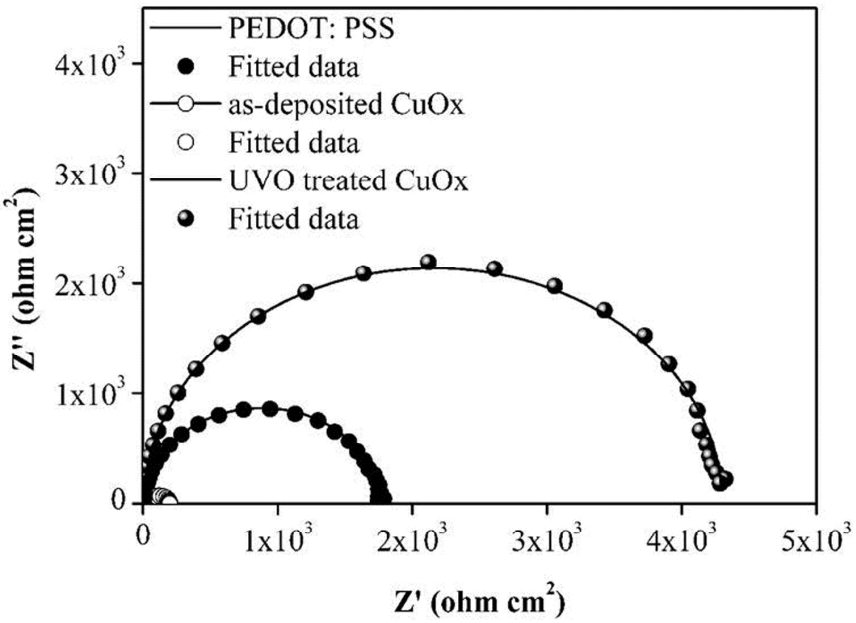

Figure 7. Nyquist plots of the PCDTBT: $PC_{71}BM$ PSCs with different anode interfacial layers.

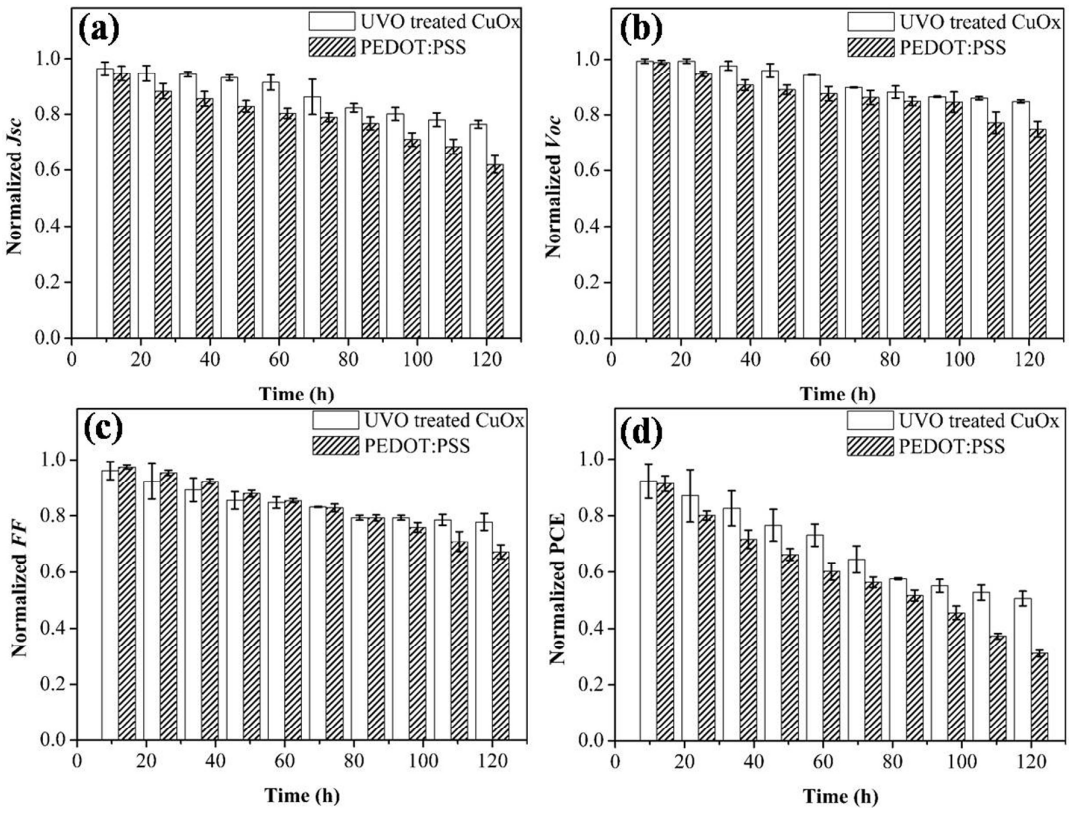

Figure 8. The degradation comparison of the normalized J_{SC} (a), V_{OC} (b), FF (c) and PCE (d) of the PCDTBT:$PC_{71}BM$ solar cells with PEDOT:PSS and the UVO-treated CuO anode buffer layers in ambient conditions.

Table 1. Photovoltaic parameters of the PCDTBT:$PC_{71}BM$ PSCs with different anode buffer layers under 100 $mWcm^{-2}$ AM1.5G simulated solar light.

Buffer layer	V_{OC} [V]	J_{SC} [mA cm^{-2}]	FF [%]	Rs[a] [Ω cm^2]	Rp[a] [Ω cm^2]	PCE [%][b]	
						best	average
As-deposited CuO	0.59	8.89	35.20	72.3	199	1.85	1.75
UVO-treated CuO	0.89	10.58	68.40	8.68	522	6.44	6.15
PEDOT:PSS	0.89	10.00	67.20	9.70	1009	6.00	5.80

[a]Series resistance (Rs) and parallel resistance (Rp) are obtained near the V_{OC} region and at around 0 V, respectively, for the PSCs under the 100 mW cm^{-2} AM1.5G simulated solar light. [b]The average PCEs were calculated over twenty devices.